Voltammetric quantification of H:Pd ratio complicated by $\alpha \leftrightarrow \beta$ phase transition in PdHx: Electrodes with low Pd loadings

Arnaud Viola, Frédéric Maillard, Galina Tsirlina

Voltammetric quantification of H:Pd ratio complicated by α↔β phase transition in PdH_x: electrodes with low Pd loadings

Arnaud Viola[1], Frédéric Maillard[1,*], Galina Tsirlina[1,2,*]

[1] University Grenoble Alpes, University of Savoie Mont Blanc, CNRS, Grenoble INP, LEPMI, 38000 Grenoble, France.

[2] CENN Nanocenter, 1000 Ljubljana, Slovenia

*** Corresponding authors**.

G.T. E-mail: Galina.Tsirlina@nanocenter.si

F.M. E-mail: frederic.maillard@grenoble-inp.fr

Abstract

The Pd hydride (PdH_x) is a typical system to study the fundamentals of solute intercalation and phase transformations or to determine the effect of strain on the rate of electrocatalytic reactions. A crucial methodological aspect, however, involves quantitatively determining the hydrogen-to-palladium atomic ratio (H:Pd) under experimental conditions where various incidental contributions to the total electrode charge are comparable to the charge spent for H adsorption/absorption and desorption. This is the case for electrodes with relatively low (dozens of $\mu g/cm^2$) loadings of Pd on various porous supports, typically used to study the oxidation of small organic molecules or the reduction of oxygen in acidic or alkaline fuel cells. Ultra-low Pd loadings (often in the range of a few $\mu g/cm^2$) are also typical for Pd nanoparticles on smooth supports, which are commonly considered as model systems for *in situ* structural studies of hydrogen sorption. To determine accurately the H content in Pd particles, we propose a technique based on analysis of charge disbalance at anodic and cathodic scans of a cyclic voltammogram, and also address the contribution of adsorbed H. To illustrate the possibilities and limitations of this technique, we present the voltametric study of thin electrodeposited Pd layers on glassy carbon and of a carbon-supported Pd catalyst.

Keywords: Hydrogen absorption; Hydrogen adsorption; Quantification of H:Pd ratio; Electrodeposition, Palladium nanoparticles.

1. Introduction

Electrochemical techniques are widely used in the studies of the famous hydrogen-palladium (H-Pd) system starting from 1950s [1–3], despite their application is limited to a narrow temperature interval. Originally seen advantage was not only a high accuracy of coulometric determination of the hydrogen-to-palladium atomic ratio (H:Pd), but also a possibility to determine the equilibrium quantities, namely the Gibbs energies of palladium hydrides (PdH_x) formation, directly from easily measured electrode potentials [1]. However, achieving equilibration of the Pd electrode in the vicinity of the α-β phase transition is challenging due to the observed hysteresis [4]. *Galvanostatic* technique with the current being intermittently interrupted, initially named 'equilibrium charging curves' (see p. 363-375 in review [3]) allows to obtain quasi-equilibrium H sorption isotherms for dispersed Pd over extended periods, often lasting several hours. The limitation of this technique comes from unavoidable presence of residual oxygen in solution. Moreover, to achieve a target adsorption/absorption-desorption charge significantly surpassing that associated with the by-side oxygen reduction reaction (ORR), a minimum of several dozen mg of Pd is necessary for electrodes of typical (*ca*. 1 cm^2) size dimensions. This is possible with Pd black, but not with Pd nanoparticles, especially for low (dozens of $\mu g/cm^2$) loadings typically used for electrocatalysis.

The same problem arises for high amplitude *potentiostatic* techniques, which assume saturation of Pd with H, and subsequent anodic extraction of H at high electrode potential: if the amount of Pd is low, the by-side charge spent for ORR can affect the result dramatically, particularly for the α-phase, characterized by its low H:Pd ratios. As an illustration, noteworthy negative H:Pd ratios were reported [5] for a 50 nm Pd film (loading of *ca*. 60 $\mu g/cm^2$), which indicates that the cathodic ORR contribution exceeded the anodic charge for H extraction. Surely the coulometry under high amplitude potential step is a powerful technique if applied to bulk metallurgical Pd samples, to say, Pd foils [1]. In addition to H:Pd ratios, this technique provides information on the movement of the boundary of α- and β-phases inside the foil saturated from one side [6]. However, this technique is unable to address equilibrium slowly establishing in the vicinity of $\alpha \leftrightarrow \beta$ phase transition [7]: the plateau in resulting isotherm is shifted to 'absorption' side of the hysteresis loop (see Figure S3b in our recent article [8]).

H extraction after potentiostatic saturation can be also done *voltammetrically*, in a single linear sweep (whereas cyclic voltammetry considered below is rarer). Combined technique of H extraction was also reported [4] (linear sweep up to ~0.5 V *vs*. reversible hydrogen electrode (RHE), and then potentiostatic extraction of residual H at the same potential). An evident advantage of voltammetry is the possibility to use the dependence on potential sweep rate for distinguishing Faradaic contributions from adsorption, absorption and desorption contributions. The former is generally independent of the potential sweep rate.

The lowest Pd loading for which Pd-H voltammetry can be found is 2 – 10 $\mu g/cm^2$ [9] (2-4 nm size Pd particles evaporated on glassy carbon [9]), which can be considered as ultra-low [10]. Most known electrochemical studies are related to essentially higher loadings. Thus, in the same period, initially inspired by discussion of 'cold fusion' [11], an extensive series of works on voltammetric quantification of H in Pd was started by Czerwinski group (the interested reader is referred to review [12]). This group names their electrodeposited 0.1 – 10 μm thick Pd layers on gold (roughly 0.1 – 10 mg/cm^2 loadings) the 'limited volume electrodes', assuming that usual samples of metallurgical Pd, *e.g*. foils, are of much higher volume. Bartlett and co-authors [13,14] studied Pd films with regular arrays of pores (0.2– 1 mg/cm^2 loadings, specific surface

area of *ca*. 90 m^2/g) fabricated by liquid crystal templated deposition. Latroche's group published very carefully done experiments [15,16] for Pd nanoparticles on high surface area carbon support, using Pd loadings of ~ 1-2 mg/cm^2. Comparative voltammetry for Pd foil and Pd deposited on gold (very wide range of loadings, starting from ca. 1.5 $\mu g/cm^2$) was reported by Lasia and co-workers [17,18].

In the majority of these works, the authors attempted to obtain H:Pd ratio at rather low sorption potentials, including negative RHE potentials. However, in these conditions, H adsorption, H absorption and hydrogen evolution processes are interfering, possibly leading to erroneous results if the latter contribution is essential. In this study, by limiting the lower potential limit to 0.02 V *vs*. RHE, we avoid the evolution of molecular hydrogen (H_2) gas and get quantitative insights into the contribution of dissolved H_2 that is generated at positive RHE potentials. The later process was noticed earlier [18–20] and described as H adatoms recombination. We accent contribution of this process to cathodic charge. As for its effect on anodic charge resulting from dissolved H_2 oxidation, the amount of H_2 formed at positive RHE potentials is much lower than under gas evolution conditions.

In what follows, we demonstrate that cathodic contribution of this Faradaic reaction, even at positive RHE potentials, should be addressed systematically in case of low Pd loadings and low enough sweep rates. To the best of our knowledge, this contribution has not been quantitatively discussed in numerous studies of the H-Pd system. Its significance is particularly pronounced in *in situ* studies involving small Pd particles, which commonly use low (a few dozens of $\mu g/cm^2$) to ultra-low (a few $\mu g/cm^2$) loadings.

2. Experimental

For solutions and electrodes preparation, H_2SO_4 (Suprapur®, Merck), HCl (Suprapur®, Merck), $PdCl_2$ (99.999 %, Acros Organics), $CuSO_4$ (Puratronic®, Thermo Scientific), 5 wt. % Nafion solution (Electrochem. Inc.), and Milli-Q water (Millipore, 18.2 MΩ cm, total organic compounds < 3 ppb) were used.

A Pd/Vulcan XC72® catalyst (Pd/C) with a nominal Pd weight fraction of 40 wt.%, mean particle diameter ~ 4 nm (**Figure S1**) was purchased from Premetek (item P30A400) and used as-received. The catalytic suspensions were prepared by ultrasonically mixing 8.2 mg of Pd/C catalyst powder (36.7 wt.% Pd, as precisely measured by inductively-coupled plasma mass spectrometry (ICP-MS)), 11 µL of 5 wt.% Nafion solution, 1446 µL of isopropanol and 3.6 mL of Milli-Q water. A 10 µL aliquot of ultrasonically-treated catalytic suspension was deposited onto a glassy carbon (GC) disk. Disc area was 0.196 cm^2, yielding a catalyst loading of *ca*. 30 $\mu g_{Pd}/cm^2$ (more precisely measured by ICP−MS after experiments, see below). A heat gun was used to evaporate the Nafion® solvents, isopropanol and water.

All measurements were done at room temperature (typically 20 ± 2°C). All potentials reported below are reported in RHE scale. RHE were filled with either 1 M HCl, or 0.5 M H_2SO_4 solutions, depending on the composition of the working electrolyte.

Pd electrodeposited samples (ED Pd) were prepared by means of potentiostatic electrodeposition from 1 wt.% $PdCl_2$ + 1 M HCl bath on anodically pre-oxidized GC disk of 0.283 cm^2 geometric area. The same deposition bath was also used in some studies of

Czerwinsky's group [21,22]. The deposition cell was equipped with a round counter electrode (Pt foil, *ca*. 12 cm^2) symmetrically located in parallel to GC surface in the same compartment. The home-made RHE ('close compartment' design) was a cylindric glass container of *ca*. 2 mL volume, with a Pt wire soldered at the top and stretched along internal part of the container. From the opposite side of the container, *ca*. 1 mm diameter opening was located, which served for the contact with external solution. RHE was charged under constant voltage mode, to accumulate H_2 gas in the upper part of the container: about a half of wire was finally located in the gas phase, and another one in solution saturated with H_2. This procedure allowed to keep stable zero RHE potential for at least 12 h. RHE was connected with the working electrode compartment via a Luggin capillary.

The support pre-treatment (5 min at 2 V in 0.5 M H_2SO_4 solution [23]) favours higher concentration of nucleation centres and improves Pd adhesion, but also increases the risk of electroless deposition. To avoid the formation of rather large Pd crystals, GC electrodes were immersed in palladium chloride bath under polarization at 0.8 V, with subsequent potential step to either 0.07, or 0.2 V deposition potential. This resulted in formation of two different morphologies, as shown in **Figure S2**. Current efficiencies were ~95 and ~100% for indicated deposition potentials, respectively. The samples with 2.5 – 35 μg/cm^2 loadings (corresponding to effective thicknesses of approximately 2 to 30 nm) were fabricated using deposition charges of up to 20 mC. In contrast to higher charges, this enabled fabrication of mechanically stable samples without peeling, and with a homogeneous morphology, as confirmed by scanning electron microscopy both after deposition and following subsequent electrochemical experiments.

The exact Pd loading in both Pd/C and ED Pd was determined using a PerkinElmer NexION 2000 ICP-MS. For the former material, a given mass of Pd/C nanocatalyst was precisely weighted and dissolved using microwave-assisted digestion (Mars 6, CEM corporation, EasyPrep Plus vessels). In detail, 3 mg of catalyst powder or 30 μL of catalytic ink were dissolved at 220°C in 10 mL of aqua regia (HNO_3:HCl 2:3). The obtained solutions were diluted with Milli-Q water, up to the final 50 mL volume. ED Pd samples (up to 10 μg Pd content) after electrochemical experiments were dissolved in 5 mL of concentrated HCl with addition of *ca*. 0.3 mL concentrated HNO_3. The solutions were diluted with Milli-Q water, up to the final 20 mL volume. Calibration curves were obtained with standard solutions, containing Pd at concentrations of 0, 5, 10, 20 and 50 μg L^{-1}, freshly prepared from mono element ICP standard solution (1000 mg L^{-1}, Carl Roth GmbH) and diluted with a 0.1 M HNO_3 solution. Rhodium was used as an internal standard.

Palladium electrodeposits tend to relax very slowly under about a dozen of subsequent potential cycles with 0.02 V cathodic limit at sweep rates of ~0.1 mV/s and lower. Relaxation is accompanied by the narrowing of the phase transition hysteresis, as well as by microstructural transformations as confirmed by X-ray diffraction experiments. We shall address this interesting phenomenon in a separate communication. Somewhat similar phenomenon was observed for much thicker deposits and much faster (10 mV/s) sweep rates in earlier studies [22,24], albeit with a significantly higher number of cycles. This observation was attributed to the emergence of structural defects. In our experiments, no signatures of relaxation were observed at sweep rates above 0.1 mV/s. All the data for ED Pd presented below are obtained without preliminary slow cycling, and the total number of CVs does not exceed 5, measured with subsequent increase of sweep rate. For preliminary stabilization of the interface, we used

cycling between 0.07 and 0.8 V, to avoid β-phase formation (the subsequent voltammograms coincided after 3-5 cycles in this interval). The slowest CVs registered in the beginning and after such a series coincide with a reasonable accuracy (peak separation decrease was *ca*. 1-2 mV, and characteristic charges remained the same with ca. 2% accuracy). Pd/C-based catalytic layers tend to faster relaxation, so the electrodes were cycled between 0.02 and 0.65 V at 5 mV/s till stable CV was obtained (typically 15-20 cycles), prior to slow cycling. The analysis of previously reported data [8] solidly confirms that the total amount of Pd remained consistent after cycling. This indicates that no peeling or dissolution takes place in this potential range.

The voltammetric experiments were conducted using a conventional glass cell equipped with a Pt counter electrode (foil of *ca.* 4 cm² geometric area) and either a commercial (Gaskatel, SKU 81010, polytetrafluorethylene body) or a home-made RHE connected with working electrode compartment via a Luggin capillary. All glassware used in this study was first cleaned with a H_2SO_4:H_2O_2 (1:1 v/v) solution overnight, then thoroughly rinsed with Milli-Q water. All H sorption data were collected in 0.5 M H_2SO_4 solution de-aerated with argon (Ar, > 99.999 %, Messer), and Ar flow above the solution was continued during all experiments. The residual oxygen in solution resulted in potential-independent (in the potential range investigated in this study, *i.e*. $E < 0.8$ V) current of 0.15-0.2 μA, and was determined with *ca*. 5% accuracy from the shift of 'double layer' region (0.4 V) at slow potential sweep rates. In the plots reported in this study, the ORR current was subtracted. All CVs were started from anodic potential limits: 0.8 V for ED Pd, and 0.7 V for Pd/C that is more prone to dissolution at high electrode potentials.

In the Cu underpotential deposition (UPD) experiments for determining the Pd real surface area, a 0.002 M $CuSO_4$ + 0.5 M H_2SO_4 solution was used. Actually, Cu UPD provides more exact values of the Pd real surface area as compared to technique based on O UPD charge [9,13,22], because it is much easier to separate UPD response and to specify the background. O UPD is useful for bulk Pd electrodes but is less suitable for Pd nanoparticles because high anodic potential limit is required. The formation of Cu adatoms on Pd is known to be slow [25] and the rate of this process can be accelerated by chloride additives [26]. However, we refrained from using chloride additives to prevent Pd dissolution. In our Cu UPD experiments, the anodic limit was set at 0.7 and 0.8 V for Pd/C and for ED Pd, respectively and the cathodic limit was set to 0.27 V. The accumulation time t_{Cu} at this potential was varied in the interval 30 – 600 s. The background CV registered in 0.5 M H_2SO_4 solution was independent of the holding time. The charge accumulated during the anodic scan (at a rate of 10 mV/s) subsequent to adatoms accumulation is spent for both the desorption of adatoms and the oxidation of Cu^+ ions generated during the holding period at 0.27 V. Correction for the contribution of Cu^+ to the anodic charge was performed through linear extrapolation, according to the procedure described in Ref. [27]. To estimate the H UPD charge, we used a half of the Cu UPD charge following the approach described in Ref. [28].

3. Results and discussion

3.1. Interplay of peaks and 'tail'

A typical sequence of CVs for ED Pd (**Figure 1**) exhibits 'triangular' features akin to those predicted for a slow phase transition [29,30] if proton discharge and diffusion processes are at (pseudo)equilibrium. Nonetheless, a qualitatively similar shape is anticipated in the case of

Ohmic contributions, and these contributions cannot be ruled out, given the conceivable decrease of PdH_x conductivity with x [31]. For ED Pd, additional resistance may also arise from the deterioration of the metal bonding to the GC support. However, we note that similar peak shape was observed also for Pd on high surface area carbon support [16],which indicates that this peak shape is intrinsic to the slow α↔β transition.

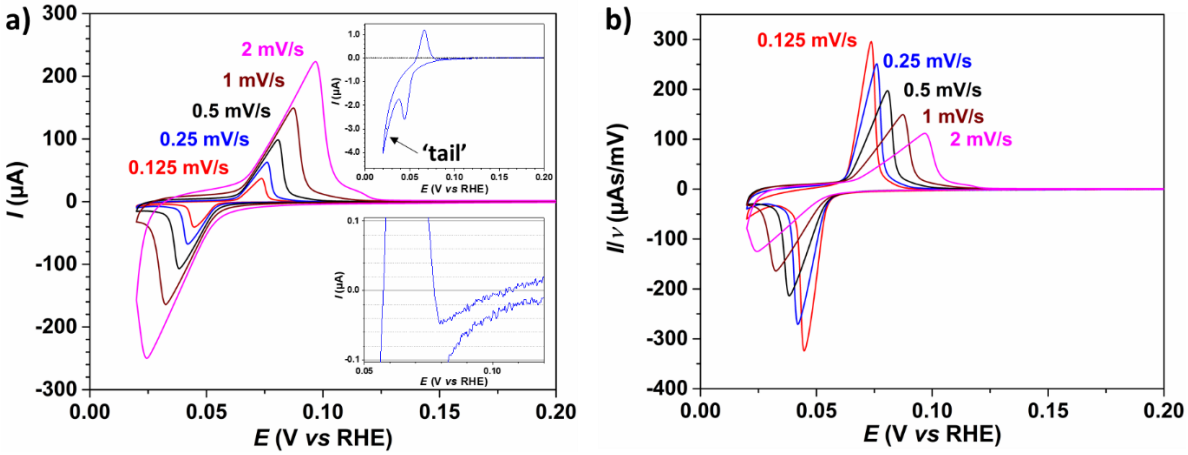

Figure 1. A series of CVs measured with subsequently increasing potential sweep rate (indicated in the plot) on ED Pd with 23.1 μg/cm^2 loading (a), and the same series with the currents normalized to sweep rate (b). Insets in plot (a) demonstrates CV for 2.4 μg/cm^2 loading at 0.125 mV/s (upper inset) and zoom for the region in which the changes of current sign are observed at anodic scan (bottom inset).

Vorotyntsev and Badiali were the first to predict the distinct voltametric manifestation of slow nucleation under phase transition conditions [29]. They developed an analytical theory for the recharging of conducting polymers. This concept is broad in scope and can be applied to different types of intercalating electrode materials. A straightforward numerical modelling can be found in the review article [32], which addresses lithium intercalation into complex oxides and accounts for contributions from solid-state diffusion and interfacial kinetics. Both these contributions are highly probable for the Pd-H system assuming the low value of H diffusion coefficient in the bulk [33] and kinetic limitations at the interface (by strongly adsorbed H) as documented in experiments with an inhibitor of H adsorption [14,18].

The potential of the middle point between the cathodic and anodic peaks, if they are symmetric enough, is 0.057 V, corresponding to ~0.01 atm effective H_2 pressure. This value is in a reasonable agreement with the equilibrium electrochemical data for α↔β-transition plateau [3], with equilibrium data obtained by potentiometric titration [34], and with the classical phase diagram of Pd-H system at room temperature [35] (~0.06 V). Nevertheless, it is approximately 0.01 V more positive compared to the phase transition values determined by means of voltammetric extraction [12,13]. The rationale remains consistent with that of potentiostatic extraction [7,29]: regardless of the extraction mode, desorption cannot be observed under purely equilibrium conditions if the phase transition is slow. As a result, the resulting data correspond to the 'absorption' branch of the hysteresis loop. In both cases, saturation and extraction potentials seem distinct due to the phase transition. We identified a single instance of transition observation between 0.05 and 0.06 V [36] for H extraction at a sweep rate of 10 mV/s from a 5 mg/cm^2 Pd/XC-72 electrode. However, considering the too fast sweep rate and the observed

decrease in charge during subsequent cycles compared to the 1st cycle, these data can scarcely be regarded as quasi-equilibrium.

Let us also emphasize that no anodic peak preceding H desorption was observed in the CVs displayed in **Figure 1**. This is in contrast to desorption curves measured after saturation at negative RHE potentials, [9,37] and reliably confirms that contribution of H_2 oxidation is absent or minimal. We nevertheless point out that a certain amount of H_2 is undoubtedly generated during the cathodic scan. This is evident in the data for low Pd loadings at low sweep rates, where a distinctive 'tail' is observed near the cathodic limit (**Figure 1a**, upper inset). This 'tail' is partly or completely masked at higher Pd loadings and faster sweep rates, where the contribution of H sorption to the total charge is sufficiently high.

The sweep rate dependence of the current at the cathodic limit (the left edge of the 'tail') is less pronounced because, at this potential, Faradaic processes predominate even at high loadings if sweep rates are low (**Figure 1a**). The experiment conducted with very low loading (see **Figure 1a**, bottom inset) enables the observation of subtle yet distinct manifestations of the 'tail' even at potentials ranging from 0.08 to 0.1 V: the total current undergoes a change in sign in this specific region. There is a prevailing belief that H_2-related Faradaic processes occur solely at negative RHE potentials [37], which holds true for the evolution of H_2 bubbles. However, it is important to note that the thermodynamic restriction against the formation of dissolved H_2 at positive RHE potentials does not apply, as long as the H_2 concentration does not exceed those determined by the corresponding effective H_2 pressure.

In the conditions of our experiments, an equilibrium between H_2 in solution and in the gas phase is never established. Consequently, the concentration of H_2 in solution remains significantly lower than the potential equilibrium concentration. It is also interesting to mention that similar ‘tail’ contribution for colloid Pd nanoparticles could be noticed starting from 0.025 V in Ref. [38]. Unfortunately, the loading conditions in this study remain uncertain, as the area of the gold support was not specified. It is reasonable to assume that 14 μg of Pd on an electrode of standard size corresponds to loadings comparable to or even higher than those investigated in our experiments. Additionally, the sweep rate in the referenced study was higher, resulting in an essential part of the ‘tail’ remaining invisible.

Last, we emphasize that for higher loadings/sweep rates cathodic currents can be observed during the anodic scan only when the potential is below approximately 0.05 V. Between approximately 0.07 and 0.1 V (refer to **Figure 1a**, bottom inset)), cathodic currents are also evident for lower loadings/lower sweep rates. The middle section of the 'tail' exhibiting these currents remains invisible, as the cathodic Faradaic process is obscured by anodic desorption of significant amounts of H in the phase transition region. Precise reconstruction of this feature is impractical, as it cannot be straightforwardly used as a 'background' for subtraction. Even the visible portion of this 'tail' contains contributions from cathodic H absorption, persisting across the overall potential range, not solely within the cathodic peak region. This persistence is attributed to the continued saturation of the β-phase, whose composition is potential-dependent, occurring after the phase transition. At higher sweep rates, saturation extends into the initial part of the anodic scan, as previously hypothesized [39]. This is closely related to the problem of uncertainty which was noticed in the study of 1-2 μm thick Pd layers on titanium supports [39]: how to account for cathodic current in anodic scan? For lower Pd loadings, the problem becomes really dramatic. Consequently, we seek a less direct approach to account for the Faradaic process, as elaborated below.

3.2. Charge disbalance and H:Pd ratio

Hypothetically, one can consider the traditional approach to separate the processes demonstrating different sweep rate dependences by means of extrapolation to either zero, or infinite sweep rate. However, we cannot access wide enough sweep rate interval experimentally because of inaccuracy of correction for ORR at very low sweep rates, and obviously incomplete H absorption at high enough sweep rates. Moreover, quantitatively, both limitations depend on Pd loading. In what follows we present a more or less universal approach for quantifying the H:Pd ratio in conditions characterized by a slow phase transition. Importantly, this method eliminates the need for extrapolation and is applicable across various Pd loadings.

Our methodological approach is based on electrical charge *vs*. potential loops obtained by integration of CVs (**Figure 2**) which include non-matching charge *vs*. potential curves for cathodic and anodic sweeps. These loops cannot be automatically considered as hysteresis induced by phase transition, as discussed in respect to critical phenomena [4]. Instead, the loops always present an interplay of hysteresis related to absorption phenomena, and the contributions from Faradaic process. Correspondingly, the shape of the loop becomes an important step of diagnostics of the latter contributions.

As depicted in **Figure 2**, a pronounced charge disbalance between cathodic and anodic charges (Q_{dis}) can be noticed. The charge disbalance (shown by vertical arrows in **Figure 2a**) is higher at lower sweep rates for any loading, and roughly proportional to the reciprocal of the sweep rate v (**Figure 3a**): visible deviations appear only at the slowest sweep rate. Please note that we consider the absolute, not relative values of Q_{dis}. Only relative Q_{dis} values were reported earlier in the literature: 5% for 0.1 mV/s sweep rate [16], and the same for much higher sweep rates [20] (to be precise, this result cannot be compared with cyclic voltammetry directly. This is because a combination of two sweeps was applied: anodic sweep after potentiostatic polarization, and then cathodic sweep). Although these relative values are seemingly small, they do not contradict our observations as they correspond to much higher Pd loadings [16,20], *i.e.* to higher total charge.

The shape of the loops varies significantly depending on the ratio of adsorption + absorption and 'tail' contributions. When the 'tail' predominates, as seen for low loadings (**Figure 2a**), the loop exhibits a less defined shape, making it difficult to determine the width of hysteresis. In cases where sorption predominates, especially at higher Pd loadings, the loop at low sweep rates displays well-defined parallel anodic and cathodic branches, accompanied by a broader asymmetric boot-like feature (as indicated by the red curves in **Figs. 2b, c**). However, at higher sweep rates, even with increased loadings, this feature is not observable due to incomplete H absorption. This shape is reminiscent of a phase transition plateau followed by a subsequent β-phase region, but it is often blurred by the hysteresis.

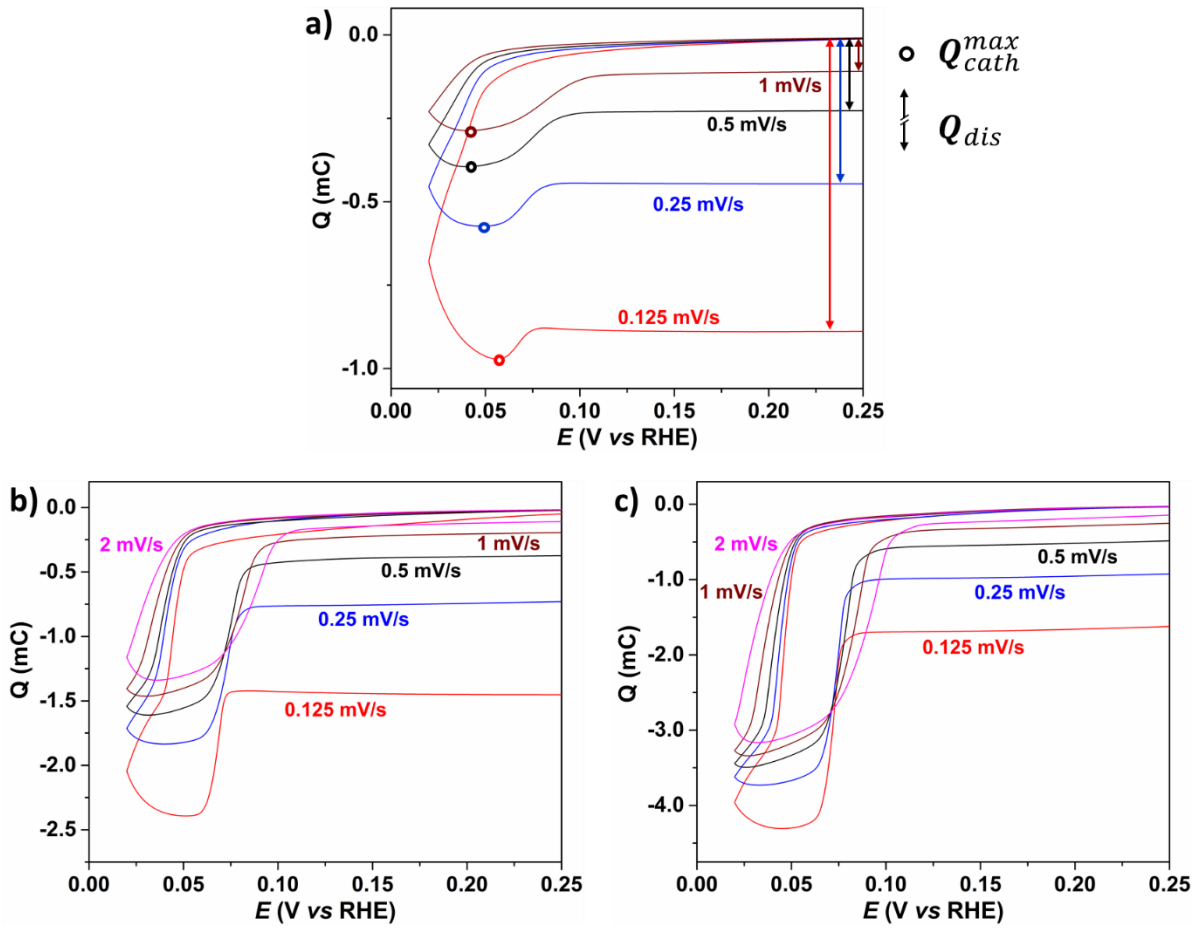

Figure 2. Charge calculated from CVs for ED Pd with the loadings of 2.4 (a), 9.2 (b), 23.1 (c) μg/cm^2. Q_{dis} (vertical arrows) and $Q_{\text{cath}}^{\text{max}}$ (open symbols) are shown as an example in Figure 2a.

Assuming that Q_{dis} is proportional (with certain accuracy) to the reciprocal of sweep rate $1/v$ (**Figure 3a**), one can assume that this quantity depends mostly on the time spent in the region of the 'tail', *i.e.* the rate of H_2 generation at any potential is the same at anodic and cathodic branches. In what follows, we explore this justified assumption. If this assertion holds true, and if the 'tail' predominantly contributes to Q_{dis} (in cases where other causes of charge disbalance, such as H_2 oxidation, hydrogen trapping, and spillover, are either absent or have a negligible impact), the charge, denoted as Q_{H}, spent for H adsorption + absorption exclusively, can be estimated using the **Equation 1**:

$$Q_{\text{H}} = |Q_{\text{cath}}^{\text{max}}| - \frac{1}{2}|Q_{\text{dis}}| \quad , \quad (1)$$

where $Q_{\text{cath}}^{\text{max}}$ is the highest observed value of the cathodic charge at this sweep rate (see open spheres in **Figure 2a** as an example). In the frame of the assumptions mentioned above, **Equation 1** is valid independently of potential at which $Q_{\text{cath}}^{\text{max}}$ is achieved. No similar procedure can be proposed for voltametric extraction because the cathodic saturation charge remains unknown.

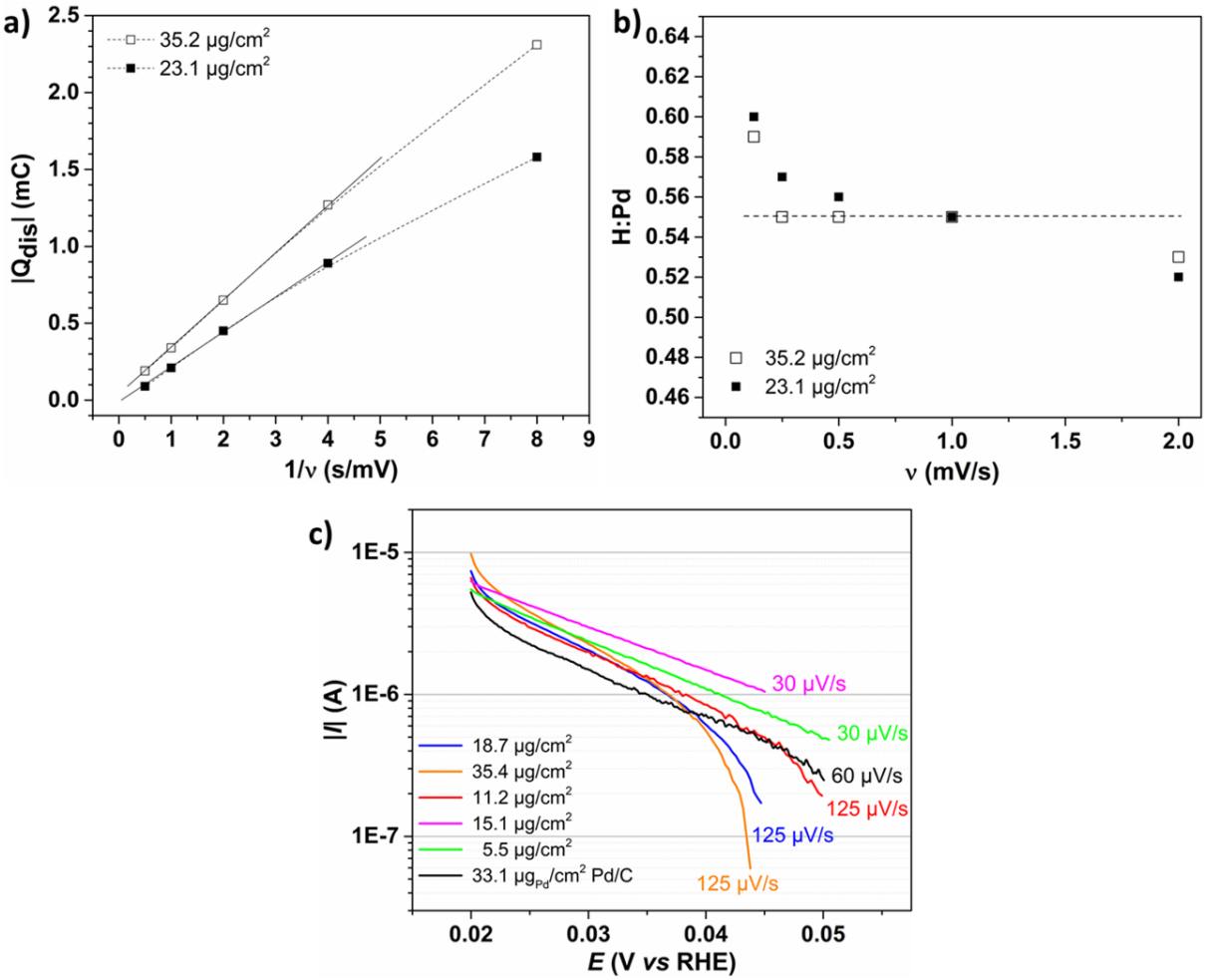

Figure 3. Sweep rate dependencies of Q_{dis} (a) and H:Pd ratio (b) calculated according to Equation 1 for ED Pd with the loadings of 23.1 (solid symbols) and 35.2 (open symbols) μg/cm^2; Tafel plots of anodic current at the 'tail' for various ED Pd samples (color curves) and Pd/C sample (black curve) (c).

The validity of the predominant 'tail' contribution can be assessed by examining the independence of the H:Pd ratio on the sweep rate. As illustrated in **Figure 3b**, the calculated Q_H using **Equation 1** yields H:Pd ratios that are indeed independent of sweep rate within a specific range, approximately ranging from 0.55 to 0.56. However, at the lowest sweep rate in the series (0.125 mV/s), the H:Pd ratios appear to be overestimated, in line with a slight deviation of the Q_{dis} *vs*. 1/*v* dependence from linearity (depicted in **Figure 3a**).

One should also note that at very low sweep rates, Q_{dis} and Q_{cath}^{max} can closely converge, casting doubt on the accuracy of subtraction. The decrease of Q_{dis} at higher sweep rates could stem from various factors. There may be an emergence of an additional anodic process, such as the oxidation of H_2, or the 'tail' current may diminish over time. The latter scenario is plausible if H_2 molecules accumulate in the solution, thereby increasing effective pressure and subsequently reducing overvoltage. In such cases, $\frac{1}{2}|Q_{dis}|$ may be lower than the quantity to be subtracted, resulting in a higher Q_H. It is also possible that at the highest sweep rate in this series (2 mV/s), the real H:Pd ratio decreases due to incomplete H absorption at the cathodic branch, as evidenced by the magenta curve in **Figure 1a** (2 mV/s) and the loop shapes in **Figure 2**.

Numerous H:Pd ratio values exceeding 0.55 can be found in the literature, primarily documented for dispersed Pd materials and discussed in the context of lattice defectiveness. Many of them (but not all) were reported for saturation potentials more negative than the zero point of the RHE. Consequently, these values may not only be genuinely higher, but also overestimated because of by-side contributions. We believe that the proposed approach only enables the distinction of anomalously high H:Pd ratios arising from genuine material characteristics, rather than from overestimations. This clarification helps to elucidate the role of Pd microstructure in its sorption properties.

The increase of anodic extraction charge at low sweep rate, reaching a subsequent maximum, was reported in Ref. [20]. This phenomenon was also qualitatively assigned to H adatoms recombination (H_2 formation), but this observation corresponds to much higher sweep rates, and also to linear (not to cyclic) voltammetry.

For Pd nanoparticles supported onto high surface area carbon, the data for slow sweep rates are rarer in the literature. For instance, a series of CVs starting from 1 mV/s and a CV at 0.1 mV/s can be found in Refs. [15] and [16], respectively. The reported values of H:Pd in these works for negative (RHE) potential limits do not exceed 0.55 – 0.60. However, they suffer from very rough subtraction procedure for H_2 oxidation reaction. Voltammetric extraction at 10 mV/s [13,14] resulted in a reasonable H:Pd value below 0.6 at positive (RHE) saturation potentials. However, the values obtained at more negative potentials seem to be overestimated. Another study reported a H:Pd ratio of 0.55 for > 3 nm Pd particles in the vicinity of the RHE zero [9] based on CV analysis at a single sweep rate of 30 mV/s. Moreover, numerous values lower than 0.55 can be found, particularly for small Pd particles/nanoparticles and were attributed to size effect (see, *e.g.* [9]). Considering 'tail' contributions (mostly screened), we can anticipate underestimated H:Pd ratios if $\frac{1}{2}|Q_{\mathrm{dis}}|$ is higher than the real 'tail' contribution to cathodic charge. This suggests that there are other factors contributing to disbalance, aside from the 'tail', which increase the Q_{dis} value. H trapping and H spillover seem to be the factors of this sort.

Figure 3c illustrates examples of 'tails' for various samples. These instances were qualitatively extracted from CVs, demonstrating the separation of the 'tail' and H absorption peak, particularly noticeable at low sweep rates. The separation becomes more pronounced with lower loadings. 'Tail' currents correlate with the real surface area as determined from Cu UPD charge (see below), but not quantitatively. This likely implies that additional contributions of H absorption, which depend on the loading and sweep rate, remain essential, at least in some cases. However, within a specific narrow potential interval, 0.02 – 0.035 V, the 'tails' exhibits Tafel behaviour with a slope of 30 – 40 mV/decade. This slope is similar to the reported 37-46 mV/decade for H_2 evolution in the range of 0 to -0.07 V [38] and slightly lower than the value reported in classical articles of Hoare and Schuldiner between -0.02 and -0.04 V RHE, 40-42 mV at comparable pH [2]. The similarity of Tafel plots supports the assignment of the 'tail' to H_2 generation.

Figure 4 presents a series of CVs featuring various cathodic limits (depicted in plot a) and their corresponding charge *vs*. potential dependencies (depicted in plot b). Sweep rate 0.5 mV/s was selected to achieve loops with a significant contribution from phase transition hysteresis, which is not possible at slower sweep rates. Simultaneously, this rate ensures complete H sorption, which is not achieved at higher sweep rates. An analysis of the charges (Q_{dis}) obtained in this series reveals an exponential relationship with the cathodic potential limit, exhibiting a sharp slope of approximately 50 mV/decade, as highlighted in the inset of **Figure 4b**. This finding

can be regarded as additional confirmation of the predominant, though not exclusive, contribution of the Faradaic process to the 'tail'. Given this observation, it is tempting to directly subtract the 'tail' and extract data for various absorption potentials from a single series of curves with a fixed cathodic limit. This procedure parallels the subtraction of steady-state H_2 evolution currents, as described in Ref. [37], and provided inaccurate H:Pd ratios of approximately ± 0.1 for loadings around ~25 and ~120 $\mu g_{Pd}/cm^2$.

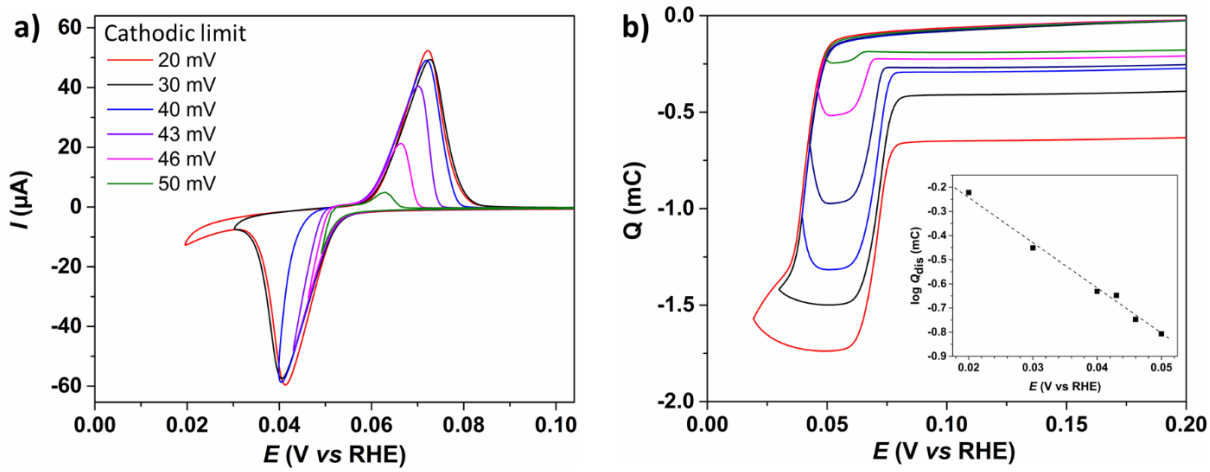

Figure 4. A series of CVs at 0.5 mV/s at various cathodic limits (a), corresponding charges (b), and the dependence of Q_{dis} on the cathodic limit for ED Pd with 9.34 $\mu g/cm^2$ loading.

Instead, H:Pd values for various β-phase potentials can be determined from a series akin to the one depicted in **Figure 4**. At this juncture, a linear H:Pd dependence was observed in the 0.02–0.04 V interval, albeit with a slope slightly deviating from previously reported slopes of the Temkin isotherm [3]. Further studies with various sweep rates are required to refine the isotherm more precisely.

If the observed loops closely resemble real phase transition hysteresis loops to a significant degree, they can provide an indication of the potential for an α↔β-transition with a certain level of accuracy. One can consider the line equidistant from anodic and cathodic branches of the loop, or the point equidistant from the anodic and cathodic peaks in slow CVs. However, similar to potentiostatic and voltammetric extraction, cyclic voltammetry does not allow for the precise determination of equilibrium H:Pd values in the closest vicinity of phase transition, even at the slowest available sweep rates. Typical width of the loops, as reported above for a 0.02 V cathodic limit, is 25-30 mV at the lowest sweep rate, and the width increases with the sweep rate (**Figure 2b,c**). An interesting observation is the narrowing of the loop when the potential of cathodic limit is increased (**Figure 4b**), *i.e.* when β-phase concentration before the start of anodic sweep decreases. This observation allows to assume that the rate of α-phase nucleation in the β-phase is higher for less concentrated β-phase. More narrow loops at the same potential limits can be observed for certain relaxed ED Pd samples, as we shall report in a separate communication.

For low Pd loadings that do not allow the determination of the loop width, the width of hysteresis region can be estimated at not too high sweep rates by considering the difference of anodic and cathodic peak potentials. Actually, for the samples/sweep rates exhibiting "well-shaped" loops, this difference coincides with the loop width within the accuracy of 1-2 mV. In

Ref. [16], a peaks separation of approximately 30 mV at a sweep rate of 0.1 mV/s was observed, consistent with our typical results. In other articles, faster CVs have been used, and peak separation is usually much higher [13,40]. It is important to mention that information on the width of phase transition region available from anodic extraction experiments cannot be compared with hysteresis loops. Czerwinsky's works typically did not analyze hysteresis [11], and the width of phase transition was estimated by examining the declined region of H:Pd *vs*. potential increase between α and β regions (see recent review [41] for additional list of articles of this group). In alkaline solutions, under conditions of simultaneous cation intercalation [24], the phase transition region was found to be considerably wide.

Another study reported a relatively narrow transition (~20 mV) for electrodeposited Pd templated by liquid crystal [13], *i.e.* for mesoporous material with ~3 nm characteristic size. This is in line with our observation of slightly wider hysteresis for Pd electrodeposited at 0.2 V, exhibiting larger crystal size (**Figure S2a, b**), compared to ED Pd fabricated at 0.07 V (**Figure S2c, d**). However, the comparison of crystallite sizes is complicated by shape differences, and the influence of deposition potential on hysteresis width for non-relaxed ED Pd is relatively small for systematic discussion. Basically, it is reasonable to assume that a decrease in size promotes a narrower hysteresis because the slow nucleation during the phase transition is linked to intercalate diffusion [32].

3.3. Electrodeposited Pd (ED Pd) versus Pd/C

The same cyclic voltammetry-based approach was applied to the commercial Pd/C catalyst featuring significantly smaller particles. Multiple CVs were recorded at varying sweep rates ranging from 60 μV/s to 10 mV/s (**Figure 5a**), revealing qualitatively similar trends as observed for ED Pd (**Figure 1**). Notably, 'tails' were discernible only at the lowest sweep rates, as illustrated above in the example in **Figure 3c** (black curve). From integration of CV curves, Q_{dis} and $Q_{\mathrm{cath}}^{\mathrm{max}}$ values were determined, as depicted in the corresponding charge *vs*. potential dependencies in **Figure 6b**.

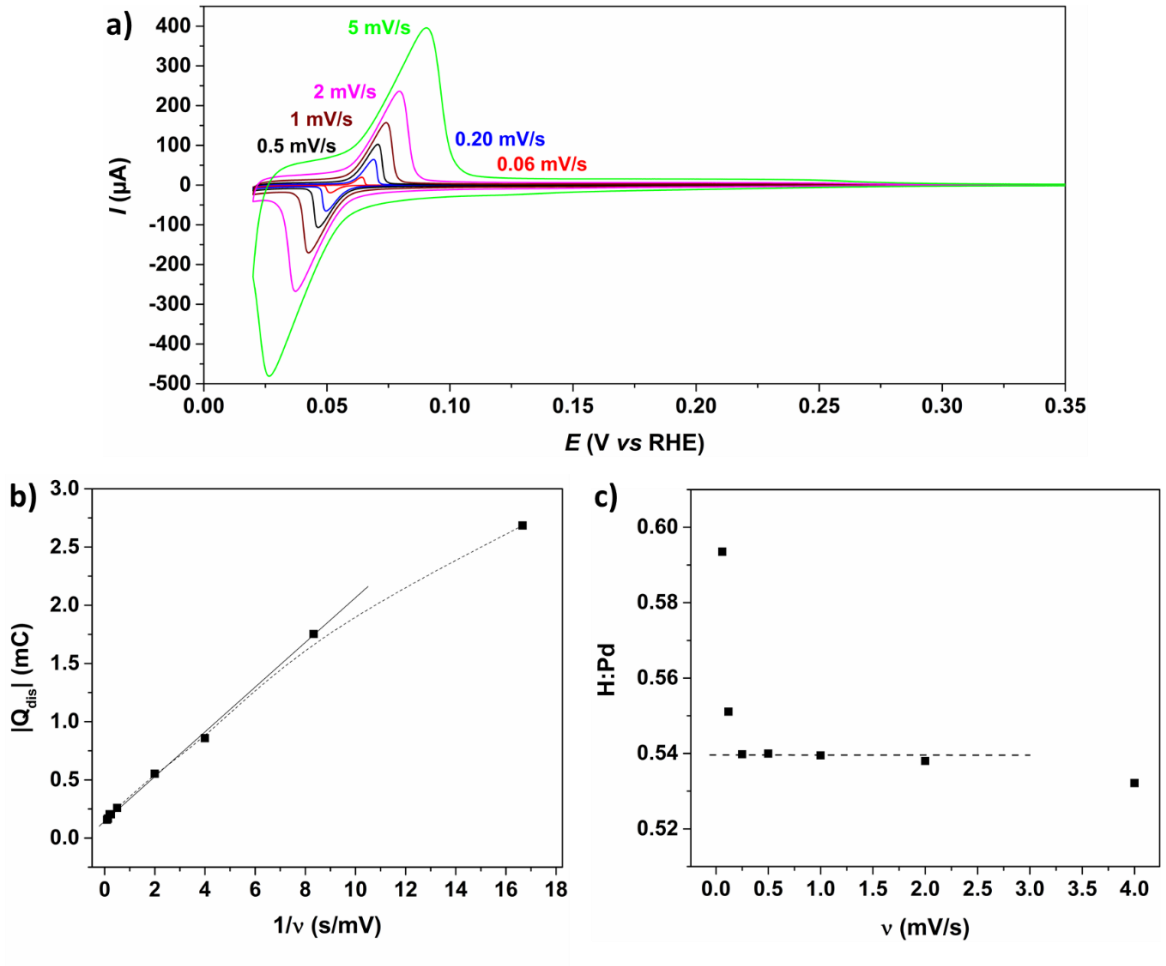

Figure 5. A series of CVs measured with subsequently increasing sweep rate (indicated in the plot) on Pd/C with 33.1 $\mu g_{Pd}/cm^2$ loading (a), charge disbalance (b), and H:Pd ratio (c) calculated according to Equation 1.

Sweep rate dependence of Q_{dis} (**Figure 5b**) appear to be linear, excluding two points for the slowest sweep rates 60 and 120 μV/s, giving a chance for identical 'tail' currents at least at all other sweep rates in a series. The H:Pd ratios, calculated according to **Equation 1** (**Figure 5c**) demonstrated sweep rate independence in a wider interval as compared to ED Pd (**Figure 3b**). Specifically, a H:Pd value of 0.54 was obtained for sweep rates comprised between 250 μV/s and 1 mV/s. The lower H:Pd values obtained for sweep rates of 2 mV/s and higher can be explained by incomplete H absorption, akin to what was observed for ED Pd. This hypothesis is supported by the shape of faster CVs in the vicinity of the cathodic limit (**Figure 5a**). Higher H:Pd at two lowest sweep rates correlate with the appearance of non-linearity of Q_{dis} *vs*. $1/\nu$ dependence (**Figure 5b**). This non-linearity suggests non-applicability of **Equation 1** under these conditions.

To compare the behaviour of ED Pd and Pd/C at various sweep rates, we present hysteresis loops for similar loadings in **Figure 6a** and **Figure 6b**, respectively. It is obvious that the hysteresis is narrower for Pd/C, and its width increases with the sweep rate for both types of materials (**Figure 6c**). The charge *vs*. potential curves displayed in **Figure 6a** do not allow to distinguish the region of H absorption in the β-phase, as it mostly screened by a wide hysteresis loop. Simultaneously, this region is quite visible in **Figure 6b** for 0.25 – 1 mV/s sweep rates, as indicated by the declined loop at 0.02 – 0.05 V. Another important feature of these curves is

the quasi-vertical shape of the loop near phase transition, reminiscent of the plateau in equilibrium absorption-desorption curves [3]. In general, the behaviour of Pd/C electrodes seems to be closer to equilibrium as compared to ED PD, especially for similar Pd loading and sweep rates, confirming that the faster diffusion in smaller Pd particles correlates with an increase in the rate of phase transition.

However, the observed difference of the curves in Figs 6a and 6b cannot be solely attributed to differences in particle sizes because Pd/C underwent relaxation during preliminary cycles, whereas ED Pd did not experience a similar relaxation. The pre-treatment of Pd/C was deemed necessary due to its quicker relaxation rate, preventing the acquisition of a sufficient number of initial cycles for non-relaxed material. For thoroughly relaxed ED Pd deposited at 0.07 V and at lower potentials, we noted a reduction in hysteresis width by up to ~15 mV at sweep rates < 0.5 mV/s. This value is already in close proximity to the reported values for Pd/C in this study. Separation of size and lattice defectiveness effects on the rate of nucleation (and probably of H diffusion in the lattice as well) is a challenging problem, which will necessitate the application of precise diffraction techniques in future studies.

The pre-treatment of Pd/C can also lead to partial H trapping, as observed earlier for a 20 wt. % Premetek Pd/C catalyst during the initial ~10 cycles [8]. If this is the case, the H:Pd ratio of 0.54 (**Figure 5c**) might be underestimated, as certain amount of H is already trapped before the start of experiment shown in **Figure 5** and **Figure 6b**. Additionally, both the ratios for ED Pd and Pd/C could be overestimated as they include contributions of charge spent for H adsorption and adatoms desorption. These contributions are addressed in the next subsection.

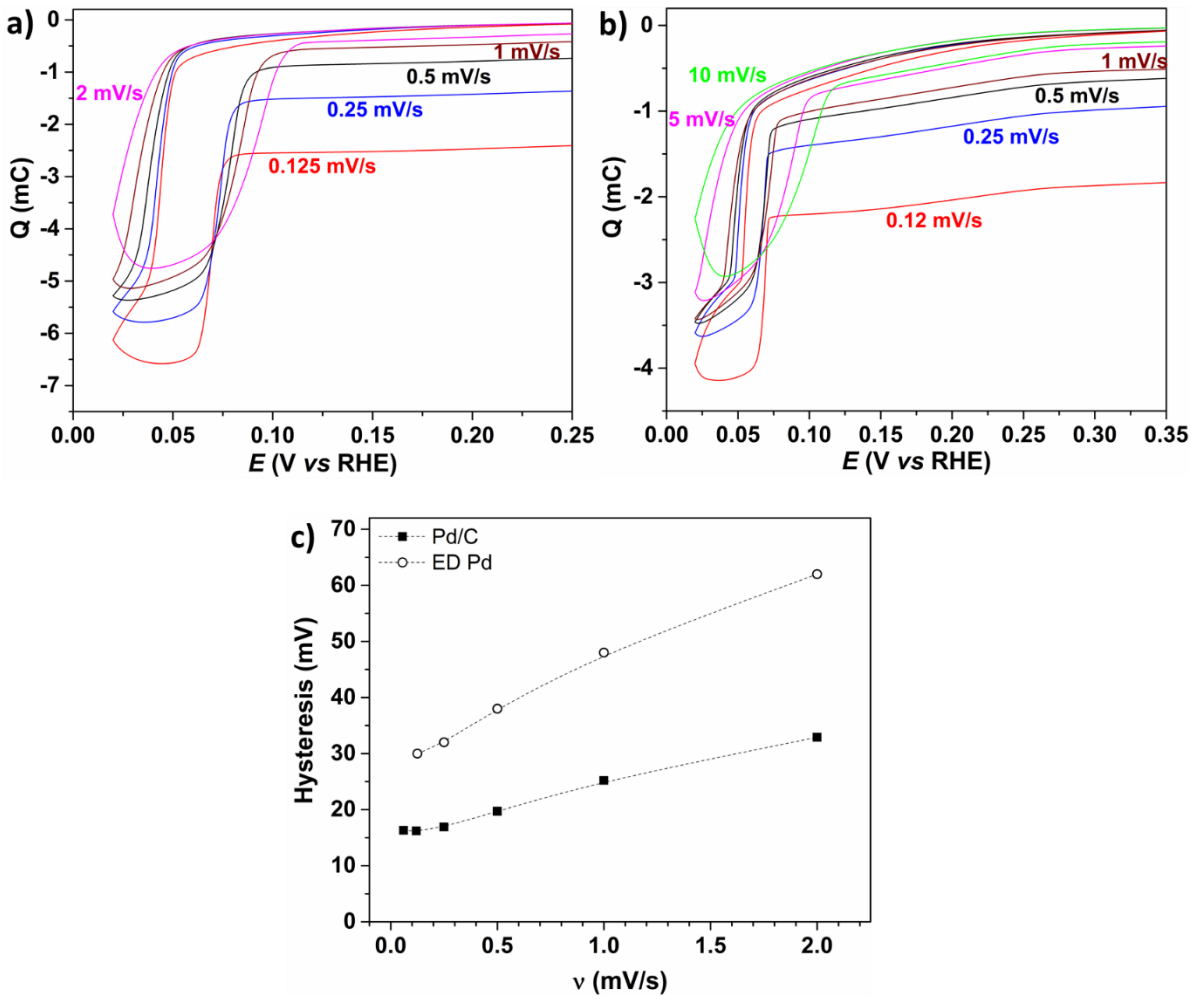

Figure. 6. Comparison of hysteresis loops for ED Pd, 35.2 μg/cm^2 (a) and Pd/C, 33.1 μg$_{Pd}$/cm^2 (b), hysteresis values are compared in plot (c). The dotted lines serve as guides to the eye.

3.4. Contribution of H adatoms and the prospects of α-phase quantification

To address the contribution of adsorbed H, we estimated the real surface area of the Pd catalysts by analysing the charge required for the desorption of Cu adatoms. A series of corresponding linear voltammograms obtained for various holding times (**Figure 7a, b**) indicates an increase in charge with holding time that is more pronounced for Pd/C. This increase could result from either slower adsorption, or a higher contribution of Cu^+, or both factors. The sluggish adsorption on Pd/C may stem from the porosity of the carbon support. Additionally, qualitative differences in UPD responses are observed. Specifically, for ED Pd (**Figure 7a**), the first desorption peak at *ca*. 0.35 V is notably higher and narrower, while Pd/C exhibits only a shoulder or a broad maximum in the vicinity of this potential. Conversely, the second peak at *ca*. 0.48 V is more pronounced for Pd/C. Notably, a distinct feature at 0.57-0.58 V is visible for ED Pd but absent for Pd/C, suggesting a significant difference in surface crystallography [26].

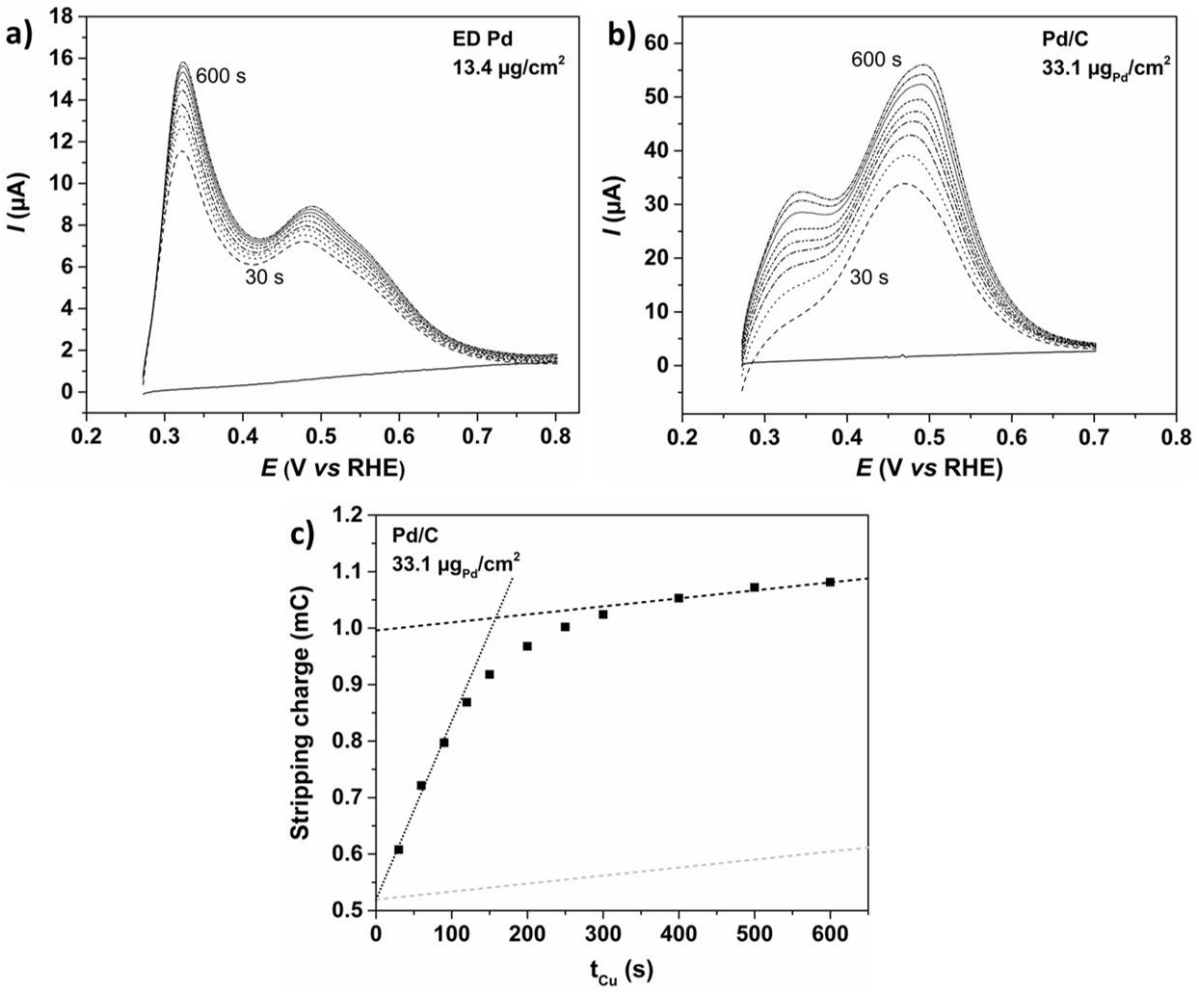

Figure 7. Cu_{UPD} stripping curves measured after various holding times, from 30 to 600s at 0.27 V for ED Pd, 13.4 µg/cm^2 (a) and Pd/C, 33.1 μg_{Pd}/cm^2 (b). The background curves (solid lines) are measured in supporting electrolyte, and are not affected by the holding time at 0.27 V. (c) Corresponding charge *vs.* holding time at 0.27 V for Pd/C.

After subtracting the Cu^+ oxidation charge (see the example of Cu^+ oxidation contribution subtraction in **Figure 7c**), the specific surface area of Pd/C was estimated to be approximately 18.3 m^2/g. This value is significantly lower than the estimation for particles of *ca*. 4 nm in size, implying particle coalescence in the Pd/C catalyst. For ED Pd, the specific surface area depends on both the deposition potential (lower for 0.2 V than for 0.07 V) and loading, although the shape of Cu desorption curves remains very similar. For instance, for samples with H:Pd ratios as presented in **Figure 3b**, the specific surface areas were 5.4 and 6.1 m^2/g. Assuming that H adatoms adsorb on the same Pd atoms as Cu UPD, we can consider half of the Cu desorption charge as the H adsorption contribution to the total charge [28]. For Pd/C as depicted in **Figure 7c**, this translates to $1/2 \times 0.48 \pm 0.03$ mC, corresponding to 0.04 on the H:Pd ratio. This implies that the H:Pd ratio for H in the Pd lattice is 0.50 instead of 0.54. For the majority of ED Pd samples, the H adsorption contribution is close to 0.01 H:Pd, slightly exceeding the accuracy of the determination of the H:Pd ratio.

The significant contribution of H adatoms to H:Pd observed in Pd/C allows to address the complex issue related to the α-phase contribution. This complexity is particularly pronounced at low loadings, where the quantities of H in the α-phase and in the H adlayer are comparable.

Previous studies have demonstrated effective separation of ad- and ab-sorbed H for Pd materials consisting of a few monolayers (loadings below 1 $\mu g_{Pd}/cm^2$) [9,13,42,43]. However, although materials with such ultralow loadings feature high surface/volume ratio, they can be hardly considered as nanoparticles due to substantial differences of their properties from those of bulk Pd. Our observations include the identification of separate broad peaks within the 0.1 - 0.28 V interval (**Figure 8a**), leading us to explore the possibility of attributing them to adsorbed H, by analogy with above-mentioned Refs.

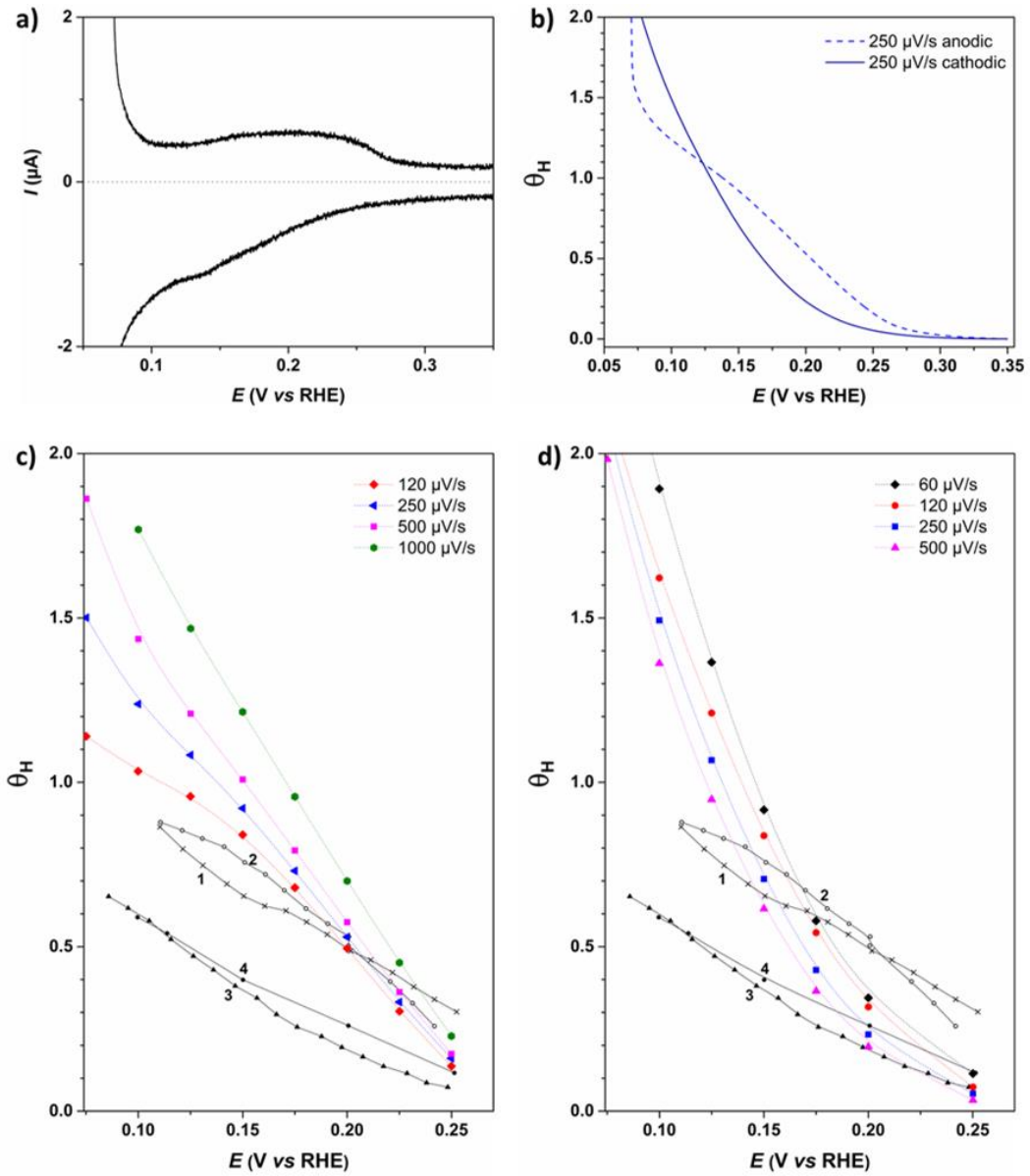

Figure 8. (a) CV of Pd/C (33.1 $\mu g_{Pd}/cm^2$) at 250 μV/s, extended region preceding phase transition; (b) H surface coverages formally calculated from the charges obtained by integration of anodic (black) and cathodic (red) branches of this CV, (c, d) comparison of calculated surface coverages (from anodic (c) and cathodic (d) branches) with hydrogen adsorption isotherms, redrawn from reference [28] (Figure 7 in Ref. [28]) for various Pd materials (1, 2 – Pd black, 3 – Pd on carbon obtained by impregnation, 4 – smooth Pd), color points correspond to potential sweep rates 60 (black), 120 (red), 250 (blue), 500 (magenta), and 1000 (green) μV/s.

Despite the fact that the region of H adsorption and α-phase formation is not complicated by phase transition, the charge versus potential dependencies do not coincide during anodic and cathodic scans, even at low sweep rates (**Figure 8b**). Quantitatively, this difference depends on the sweep rate. In **Figure 8b**, we normalized the charge to the H monolayer formation charge determined from Cu UPD to obtain H surface coverage (θ_H) and found that the values exceed 1 starting from 0.12 – 0.15 V. However, θ_H at these potentials is expected to be below one monolayer [28]. To analyse more precisely, we compared θ_H values for various potentials with the values reported earlier [28] for various Pd materials. The experiments presented in Ref. [28] consisted of comparing data for a pure Pd surface and a surface poisoned with Cu adatoms, so θ_H values were obtained by subtracting the latter from the former. Coloured points in **Figure 8c** and **Figure 8d** show our θ_H values, which are sweep rate-dependent. Despite this uncertainty, we can conclude that during the cathodic scan (**Figure 8d**), the amount of sorbed H starts to exceed the equilibrium amount of H adatoms at the lowest potential of 0.15 V. During the anodic scan, the charge can be assigned to the equilibrium amount of H adatoms starting only from 0.2 V. This result demonstrates an evident overlap of adsorption and α-phase formation and also allows us to assume that the α-phase in Pd/C starts to form at high enough potentials (0.15 V translating into approximately 10^{-5} atm effective H_2 pressure). Moreover, at an approximately 0.075 V, formally calculated θ_H approaches 2, indicating that the quantity of H in the α-phase is the same as in the adlayer (H:Pd ~ 0.04). This quantity is evidently even higher in the vicinity of the phase transition. We can assume that this is typical for Pd nanoparticles, which are known to feature a decrease in β-phase H concentration with a simultaneous increase in H content in the α-phase [44]. A more precise analysis of α-phase behaviour requires a very careful separation of 'double layer' contributions, which is complicated by the presence of foreign support. In any case, we can conclude that the α-phase overlaps with both adsorbed H and β-phase. We cannot exclude that the degree of this overlap depends on particle size and other factors, but the immediate assignment of peaks seems to be very debatable. For example, two peaks were assigned to H desorption from α- and β-phases [36], but the separation can be of kinetic nature as well. At least approximate estimates of H adatoms' contribution will be helpful to solve this quest.

3.5. Concluding remarks

Electrochemical quantification of the H:Pd ratio and determination of the phase transition region are crucial aspects in the research of Pd nanomaterials, given the limited availability of alternative tools. Estimating the H:Pd ratio from the lattice parameter [45], as outlined in a systematic study [46], offers fewer options for studying the microstructural effects of H in Pd at elevated temperatures, as lattice relaxation may lag behind H desorption [8]. Quartz crystal microbalance data, independent of coulometry, do not correlate due to the stress induced by H sorption affecting quartz resonance [47], with the effect strongly contingent on the microstructure of the Pd material.

The approach described in this study, involving cyclic voltammetry and the analysis of charge disbalance, seeks to identify a sweep rate interval where specific assumptions are applicable. This interval may vary for materials containing Pd particles of different sizes. However, the data analysis becomes more intricate as the Pd loading decreases. Generally, this approach can be effective, with certain limitations, for saturation potentials lower than 0.02 V *vs*. RHE. This is feasible for loadings not too low (starting from several dozens of $\mu g/cm^2$) and under convection modes, aiming to avoid a significant contribution from molecular H_2 oxidation. We stress that choosing very low saturation potentials, such as -1.5 V *vs*. RHE [5], is not advisable, and gives no chance even to approach equilibrium (effective pressure is already dramatically lower than predicted by Nernst equation). In addition, doing so tends to

overestimate the H:Pd value due to the unavoidable contribution from the oxidation of evolved H_2 gas at the cathodic limit, even in advanced flow cell configurations.

Comparative results for aqueous and polymer electrolyte systems [46] demonstrate that, even at negative RHE potentials, the actual H:Pd value rarely exceeds 0.8. This is no surprise, as the Nernst relationship between potential and effective H_2 pressure fails to operate in the absence of equilibrium. Therefore, the notion of holding H:Pd ~1 in typical Pd materials is illusory. This does not discount the possibility of high H:Pd ratios in specific highly defective Pd materials but is more plausible at reasonable potentials.

Formation of H_2 at positive RHE potentials is the rationale behind the recommendation to initiate experiments from a small positive RHE potential, rather than starting from zero, when determining the real surface area of platinum (Pt) [48]. Gilman [49] addressed the challenge of charge separation for Faradaic process and adsorbed H. Dealing with the rapid H adsorption process on Pt, a broad range of sweep rates, including very fast rates, could be employed. However, this flexibility is not applicable to H absorption by Pd, which is incomplete starting from certain sweep rates. Assuming the kinetical aspect, this situation is partly similar to cations intercalation into battery materials, but even more complex, as no stoichiometry limit can be reached in available potential interval. Under these complex circumstances, our alternative approach (despite its limitations) can be widely applied to various Pd materials.

We demonstrated that our experimental approach is particularly relevant for ultralow Pd loadings (of the order of 1 $\mu g/cm^2$), a characteristic of several intriguing Pd model materials [38,40,42,43,50–52]. It is also significant for foils [53], typically unable to be fully saturated with H due to diffusion limitations, resulting in a lower total absorption charge. While flow cells and electrode rotation [1,45,54] are helpful under gas evolution conditions, their combination with standard extraction procedures exclusively eliminates H_2 contribution to the anodic charge. The 'proton pump' [55,56] could potentially be a viable option with further development for more precise potential measurements.

Our approach gains special importance in deuterium absorption [57], where the isotope effect shifts the phase transition to lower potentials, making the contribution of the 'tail' crucial even at moderate loadings. A dedicated study is needed to assess the applicability of the approach to H sorption in alkaline solutions, where complications arise from cation intercalation [19].

Another crucial, though less in vogue, issue is the quantification of the α-phase, particularly challenging for Pd on supports with high 'double layer' capacity. Potentiostatic and voltametric extraction remains pivotal for the α-phase [21], especially when the absorption potential exceeds 0.08-0.09 V *vs*. RHE, and the contribution of H_2 generation is negligible. Combining disbalance analysis with extraction from the α-phase offers a detailed description of all absorption phenomena in the H-Pd system.

Insights from *in situ* structural research remain valuable, even if H:Pd ratios are determined with less precision. This information is expected to be even more valuable with the prospect of a more quantitative characterization of PdH_x composition.

4. Conclusions

The quantification of the H:Pd atomic ratio, based on an analysis of charge disbalance in a series of cyclic voltammograms, is presented for Pd loadings ranging from 2.5 to 35 $\mu g/cm^2$ on glassy carbon and Vulcan XC72 carbon supports. Sweep rate dependences for charge disbalance reveal

the range of sweep rates where the side contribution of the Faradaic reaction (molecular H_2 formation) predominates over other side processes. Under these conditions, the current associated with molecular H_2 formation remains identical during both anodic and cathodic scans, eliminating the need for precise separation of the Faradaic process.

This favourable scenario is identified through the linear relationship between charge disbalance and the reciprocal of the sweep rate, further confirmed by the independence of the calculated H:Pd ratio from the sweep rate. In the case of dispersed Pd materials studied, both criteria were met within the 0.2–1 mV/s sweep rate interval. The proposed technique also facilitates an accurate estimation of the equilibrium $\alpha \leftrightarrow \beta$ phase transition potential, even in the presence of non-equilibrium charging near the phase transition.

The proposed approach can be supplemented by analysis of H adsorption and α-phase composition, to result in complete characterization of hydrogen-palladium behaviour for complex materials with low Pd loadings.

CRediT authorship contribution statement

Arnaud Viola: Sample collection and analysis; Investigation; Formal analysis; Drawing; Data curation; Writing – review & editing. **Galina Tsirlina**: Conceptualization; Methodology, Investigation; Sample collection and analysis; Formal analysis; Drawing; Data curation; Writing – original draft; Writing – review & editing. **Frédéric Maillard**: Data curation; Funding acquisition; Resources; Validation; Writing – review & editing.

Declaration of competing interest

The authors declare that they have no known competing financial interests or personal relationships that could have appeared to influence the work reported in this paper.

Appendix A. Supporting information

Supplementary data associated with this article can be found in the online version at DOI.

Acknowledgements

This study received funding from the European Union's Horizon 2020 research and innovation program under grant agreement HERMES Nº 952184. GT is grateful to Pause program, U. Grenoble Alpes and HERMES for support of her stay at LEPMI. We thank M. Vincent Martin for ICP-MS analyses.

References

[1] T.B. Flanagan, F.A. Lewis, Electrode potentials of the palladium + hydrogen system, Trans. Faraday Soc. 55 (1959) 1409–1420. https://doi.org/10.1039/tf9595501409.

[2] J.P. Hoare, S. Schuldiner, Effects of hydrogen content on the resistance and the potential in the palladium-hydrogen-acid system, J. Phys. Chem. 61 (1957) 399–402.

https://doi.org/10.1021/j150550a004.

[3] A.N. Frumkin, Hydrogen overvoltage and adsorption phenomena. Part II., in: Adv. Electrochem. Sci. Eng. , Interscience Publ, NY-London, 1963: pp. 287–389.

[4] F.A. Lewis, The palladium-hydrogen system: Structures near phase transition and critical points, Int. J. Hydrogen Energy. 20 (1995) 587–592. https://doi.org/10.1016/0360-3199(94)00113-E.

[5] A.T. Landers, H. Peng, D.M. Koshy, S.H. Lee, J.T. Feaster, J.C. Lin, J.W. Beeman, D. Higgins, J. Yano, W.S. Drisdell, R.C. Davis, M. Bajdich, F. Abild-Pedersen, A. Mehta, T.F. Jaramillo, C. Hahn, Dynamics and hysteresis of hydrogen intercalation and deintercalation in palladium electrodes: A multimodal *in situ* X-ray diffraction, coulometry, and computational study, Chem. Mater. 33 (2021) 5872–5884. https://doi.org/10.1021/acs.chemmater.1c00291.

[6] P. Millet, M. Srour, R. Faure, R. Durand, A study of the hydrogen absorption and desorption reactions in palladium electrodes using the potential step method, Electrochem. Commun. 3 (2001) 478–482. https://doi.org/10.1016/S1388-2481(01)00190-4.

[7] D. Aurbach, M.D. Levi, E. Levi, A review on the solid-state ionics of electrochemical intercalation processes: How to interpret properly their electrochemical response, Solid State Ionics. 179 (2008) 742–751. https://doi.org/10.1016/j.ssi.2007.12.070.

[8] A. Viola, R. Chattot, V. Martin, G. Tsirlina, J. Nelayah, J. Drnec, F. Maillard, Hydrogen trapping in palladium nanoparticles revealed by electrochemical, X-ray scattering, and spectrometric measurements, J. Phys. Chem. C. 127 (2023) 17761–17769. https://doi.org/10.1021/acs.jpcc.3c04464.

[9] N. Tateishi, K. Yahikozawa, K. Nishimura, S. Masato, Y. Iwanaga, M. Watanabe, E. Enami, Y. Matsuda, Y. Takasu, Electrochemical properties of ultra-fine palladium particles for adsorption and absorption of hydrogen in an aqueous $HClO_4$ solution, Electrochim. Acta. 36 (1991) 1235–1240. https://doi:10.1016/0013-4686(91)85114-M.

[10] F. Guo, T.J. Macdonald, A.J. Sobrido, L. Liu, J. Feng, G. He, Recent advances in ultralow-Pt-loading electrocatalysts for the efficient hydrogen evolution, Adv. Sci. 10 (2023) 2301098. https://doi.org/10.1002/advs.202301098.

[11] A. Czerwiński, R. Marassi, S. Zamponi, The absorption of hydrogen and deuterium in thin palladium electrodes. Part I. Acidic solutions, J. Electroanal. Chem. 316 (1991) 211–221. https://doi.org/10.1016/0022-0728(91)87047-8.

[12] M. Łukaszewski, A. Czerwiński, The method of limited volume electrodes as a tool for hydrogen electrosorption studies in palladium and its alloys, J. Solid State Electrochem. 15 (2011) 2489–2522. https://doi.org/10.1007/s10008-011-1506-5.

[13] P.N. Bartlett, B. Gollas, S. Guerin, J. Marwan, The preparation and characterisation of H1-e palladium films with a regular hexagonal nanostructure formed by electrochemical deposition from lyotropic liquid crystalline phases, Phys. Chem. Chem. Phys. 4 (2002) 3835–3842. https://doi.org/10.1039/b201845d.

[14] P.N. Bartlett, J. Marwan, The effect of surface species on the rate of H sorption into nanostructured Pd, Phys. Chem. Chem. Phys. 6 (2004) 2895–2898. https://doi.org/10.1039/b404028g.

[15] C. Cachet-Vivier, S. Bastide, M. Laurent, C. Zlotea, M. Latroche, Hydrogen sorption

properties of Pd nanoparticles dispersed on graphitic carbon studied with a cavity microelectrode, Electrochim. Acta. 83 (2012) 133–139. https://doi.org/10.1016/j.electacta.2012.08.037.

[16] S. Bastide, C. Zlotea, M. Laurent, M. Latroche, C. Cachet-Vivier, Direct assessment from cyclic voltammetry of size effect on the hydrogen sorption properties of Pd nanoparticle/carbon hybrids, J. Electroanal. Chem. 706 (2013) 33–39. https://doi.org/10.1016/j.jelechem.2013.07.036.

[17] H. Duncan, A. Lasia, Separation of hydrogen adsorption and absorption on Pd thin films, Electrochim. Acta. 53 (2008) 6845–6850. https://doi.org/10.1016/j.electacta.2007.12.012.

[18] L. Birry, A. Lasia, Effect of crystal violet on the kinetics of H sorption into Pd, Electrochim. Acta. 51 (2006) 3356–3364. https://doi.org/10.1016/j.electacta.2005.09.034.

[19] A. Czerwiński, I. Kiersztyn, M.S. Grdeń, Study of hydrogen sorption in palladium limited volume electrodes (Pd-LVE). Part II. Basic solutions, J. Electroanal. Chem. 492 (2000) 128–136. https://doi.org/10.1016/S0022-0728(00)00291-6.

[20] A. Czerwiński, I. Kiersztyn, M.S. Grdeń, J. Czapla, Study of hydrogen sorption in palladium limited volume electrodes (Pd-LVE). I. Acidic solutions, J. Electroanal. Chem. 471 (1999) 190–195. https://doi.org/10.1016/S0022-0728(99)00276-4.

[21] M.Y. Rusanova, M. Grden, A. Czerwinski, G.A. Tsirlina, O.A. Petrii, T.Y. Safonova, Isotope effects in α-PdH(D) as an instrument for diagnosing bulk defects, J. Solid State Electrochem. 5 (2001) 212–220. https://doi.org/10.1007/s100080000135.

[22] K. Hubkowska, M. Soszko, M. Symonowicz, M. Łukaszewski, A. Czerwiński, Electrochemical behavior of a Pd thin film electrode in concentrated alkaline media, Electrocatalysis. 8 (2017) 295–300. https://doi.org/10.1007/s12678-017-0379-5.

[23] O. V Sherstyuk, S.N. Pron'kin, A.L. Chuvilin, A.N. Salanov, E.R. Savinova, G.A. Tsirlina, O.A. Petrii, Platinum electrodeposits on glassy carbon: The formation mechanism, morphology, and adsorption properties, Russ. J. Electrochem. 36 (2000) 741–751. https://doi.org/10.1007/BF02757674.

[24] A. Czerwiński, J. Frydrych, I. Kiersztyn, Influence of rubidium cations on hydrogen and deuterium electrosorption in palladium, Anal. Lett. 29 (1996) 2549–2561. https://doi.org/10.1080/00032719608002791.

[25] T. Chierchie, C. Mayer, Voltammetric study of the underpotential deposition of copper on polycrystalline and single crystal palladium surfaces, Electrochim. Acta. 33 (1988) 341–345. https://doi.org/10.1016/0013-4686(88)85026-6.

[26] E. Garnier, F.J. Vidal-Iglesias, J.M. Feliu, J. Solla-Gullón, Surface structure characterization of shape and size controlled Pd nanoparticles by Cu UPD: A quantitative approach, Front. Chem. 7 (2019) 527. https://doi.org/10.3389/fchem.2019.00527.

[27] L. Rabinovich, O. Lev, G.A. Tsirlina, Electrochemical characterization of Pd modified ceramic|carbon electrodes: Partially flooded versus wetted channel hydrophobic gas electrodes, J. Electroanal. Chem. 466 (1999) 45–59. https://doi.org/10.1016/S0022-0728(99)00118-7.

[28] B.I. Podlovchenko, E.A. Kolyadko, S. Lu, Specific features of hydrogen sorption by

palladium dispersed forms at α-phase potentials, J. Electroanal. Chem. 399 (1995) 21–27. https://doi.org/10.1016/0022-0728(95)04040-4.

[29] M.A. Vorotyntsev, J.P. Badiali, Short-range electron-ion interaction effects in charging the electroactive polymer films, Electrochim. Acta. 39 (1994) 289–306. https://doi.org/10.1016/0013-4686(94)80064-2.

[30] W.S. Zhang, X.W. Zhang, X.G. Zhao, Voltammograms of thin layer Pd | H(D) electrodes in the coexistence of α and β phases, J. Electroanal. Chem. 458 (1998) 107–112. https://doi.org/10.1016/S0022-0728(98)00350-7.

[31] S. Wagner, A. Pundt, Electrical resistivity and hydrogen solubility of PdH_c thin films, Acta Mater. 58 (2010) 1387–1394. https://doi.org/10.1016/j.actamat.2009.10.045.

[32] V.A. Nikitina, S.Y. Vassiliev, K.J. Stevenson, Metal-ion coupled electron transfer kinetics in intercalation-based transition metal oxides, Adv. Energy Mater. 10 (2020) 1903933. https://doi.org/10.1002/aenm.201903933.

[33] J. Völkl, G. Alefeld, Diffusion of hydrogen in metals, in: G. Alefeld, J. Völkl (Eds.), Hydrog. Met. I Basic Prop., Springer Berlin Heidelberg, Berlin, Heidelberg, 1978: pp. 321–348. https://doi.org/10.1007/3540087052_51.

[34] T. Imokawa, K.-J. Williams, G. Denuault, Fabrication and characterization of nanostructured Pd hydride pH microelectrodes, Anal. Chem. 78 (2006) 265–271. https://doi.org/10.1021/ac051328j.

[35] H. Frieske, E. Wicke, Magnetic susceptibility and equilibrium diagram of PdH_n, Ber. Bunsen. Phys. Chem. (Phys. Chem. Chem. Phys.). 77 (1973) 48–52. https://doi.org/https://doi.org/10.1002/bbpc.19730770112.

[36] A. Rose, S. Maniguet, R.J. Mathew, C. Slater, J. Yao, A.E. Russell, Hydride phase formation in carbon supported palladium nanoparticle electrodes investigated using in situ EXAFS and XRD, Phys. Chem. Chem. Phys. 5 (2003) 3220–3225. https://doi.org/10.1039/b302956e.

[37] B. Wickman, M. Fredriksson, L. Feng, N. Lindahl, J. Hagberg, C. Langhammer, Depth probing of the hydride formation process in thin Pd films by combined electrochemistry and fiber optics-based in situ UV/vis spectroscopy, Phys. Chem. Chem. Phys. 17 (2015) 18953–18960. https://doi.org/10.1039/c5cp01339a.

[38] A. Zalineeva, S. Baranton, C. Coutanceau, G. Jerkiewicz, Electrochemical behavior of unsupported shaped palladium nanoparticles, Langmuir. 31 (2015) 1605–1609. https://doi.org/10.1021/la5025229.

[39] C.C. Hu, T.C. Wen, Voltammetric investigation of hydrogen sorption/desorption at/within oxide-derived Pd electrodes in NaOH and H_2SO_4, J. Electrochem. Soc. 141 (1994) 2996–3001. https://doi.org/10.1149/1.2059271.

[40] G.R. Stafford, U. Bertocci, In situ stress and nanogravimetric measurements during hydrogen adsorption/absorption on Pd overlayers deposited onto (111)-textured Au, J. Phys. Chem. C. 113 (2009) 13249–13256. https://doi.org/10.1021/jp902382q.

[41] K. Hubkowska, M. Pająk, D. Monikowska, A. Czerwiński, Pd-H as an irreplaceable model system for the study of hydrogen electrosorption in aqueous and non-aqueous electrolytes, J. Solid State Electrochem. 28 (2024) 1159-1169. https://doi.org/10.1007/s10008-024-05799-5.

[42] M. Baldauf, D.M. Kolb, A hydrogen adsorption and absorption study with ultrathin Pd

overlayers on Au(111) and Au(100), Electrochim. Acta. 38 (1993) 2145–2153. https://doi.org/10.1016/0013-4686(93)80091-D.

[43] L.A. Kibler, A.M. El-Aziz, D.M. Kolb, Electrochemical behaviour of pseudomorphic overlayers: Pd on Au(1 1 1), J. Mol. Catal. A Chem. 199 (2003) 57–63. https://doi.org/10.1016/S1381-1169(03)00018-9.

[44] S. Dekura, H. Kobayashi, K. Kusada, H. Kitagawa, Hydrogen in palladium and storage properties of related nanomaterials: Size, shape, alloying, and metal-organic framework coating effects, Chemphyschem. 20 (2019) 1158–1176. https://doi.org/10.1002/cphc.201900109.

[45] R. Chattot, I. Martens, M. Mirolo, M. Ronovsky, F. Russello, H. Isern, G. Braesch, E. Hornberger, P. Strasser, E. Sibert, M. Chatenet, V. Honkimaki, J. Drnec, Electrochemical strain dynamics in noble metal nanocatalysts, J Am Chem Soc. 143 (2021) 17068–17078. https://doi.org/10.1021/jacs.1c06780.

[46] J.D. Benck, A. Jackson, D. Young, D. Rettenwander, Y.M. Chiang, Producing high concentrations of hydrogen in palladium via electrochemical insertion from aqueous and solid electrolytes, Chem. Mater. 31 (2019) 4234–4245. https://doi.org/10.1021/acs.chemmater.9b01243.

[47] M. Grdeń, J. Kotowski, A. Czerwiński, Study of electrochemical palladium behavior by the quartz crystal microbalance. I. Acidic Solutions, J. Solid State Electrochem. 3 (1999) 348–351. https://doi.org/10.1007/s100080050165.

[48] S. Trasatti, O.A. Petrii, International union of pure and applied chemistry physical chemistry division commission on electrochemistry: Real surface area measurements in electrochemistry, Pure Appl. Chem. 63 (1991) 711–734. https://doi.org/10.1351/pac199163050711.

[49] S. Gilman, Measurement of hydrogen adsorption by the multipulse potentiodynamic (mpp) method, J. Electroanal. Chem. 7 (1964) 382–391. https://doi.org/10.1016/0022-0728(64)80026-7.

[50] M. Favaro, S. Agnoli, L. Perini, C. Durante, A. Gennaro, G. Granozzi, Palladium nanoparticles supported on nitrogen-doped HOPG: A surface science and electrochemical study, Phys. Chem. Chem. Phys. 15 (2013) 2923–2931. https://doi.org/10.1039/c2cp44154c.

[51] W. Ju, T. Brülle, M. Favaro, L. Perini, C. Durante, O. Schneider, U. Stimming, Palladium nanoparticles supported on highly oriented pyrolytic graphite: Preparation, reactivity and stability, ChemElectroChem. 2 (2015) 547–558. https://doi.org/10.1002/celc.201402379.

[52] L.B. Sheridan, D.K. Gebregziabiher, J.L. Stickney, D.B. Robinson, Formation of palladium nanofilms using electrochemical atomic layer deposition (E-ALD) with chloride complexation, Langmuir. 29 (2013) 1592–1600. https://doi.org/10.1021/la303816z.

[53] J.N. Han, J.W. Lee, M. Seo, S.I. Pyun, Analysis of stresses generated during hydrogen transport through a Pd foil electrode under potential sweep conditions, J. Electroanal. Chem. 506 (2001) 1–10. https://doi.org/10.1016/S0022-0728(01)00481-8.

[54] R.S. Sherbo, M. Moreno-Gonzalez, N.J.J. Johnson, D.J. Dvorak, D.K. Fork, C.P. Berlinguette, Accurate coulometric quantification of hydrogen absorption in palladium nanoparticles and thin films, Chem. Mater. 30 (2018) 3963–3970.

https://doi.org/10.1021/acs.chemmater.8b01324.

[55] L. Moumaneix, A. Rautakorpi, T. Kallio, Interactions between hydrogen and palladium nanoparticles: Resolving adsorption and absorption contributions, ChemElectroChem. 10 (2023) e202201109. https://doi.org/10.1002/celc.202201109.

[56] L. Moumaneix, A. Rautakorpi, T. Kallio, Controlling the reactivity and interactions between hydrogen and palladium nanoparticles via management of the particle diameter, ChemElectroChem. 10 (2023) e202300111. https://doi.org/10.1002/celc.202300111.

[57] A. Rose, O. South, I. Harvey, S. Diaz-Moreno, J.R. Owen, A.E. Russell, In situ time resolved studies of hydride and deuteride formation in Pd/C electrodes via energy dispersive X-ray absorption spectroscopy, Phys. Chem. Chem. Phys. 7 (2005) 366–372. https://doi.org/10.1039/b412066c.